JOURNAL OF MATERIALS SCIENCE: MATERIALS IN MEDICINE 1 (1990) 94–99

The mould-filling capacity of two casting alloys

H. HERØ
NIOM, Scandinavian Institute of Dental Materials, Haslum, Norway

The mould-filling capacities of an Au–Ag–Cu alloy and a Ni–Cr–Be alloy for dental use have been studied by measuring the lengths of cast helices of a constant cross-section as a function of the supertemperature of the melt. A vacuum–pressure casting machine was applied in the experiments. Assuming that the conduction of heat through the investment is rate-controlling for the heat flow, the heat of fusion was calculated for the two alloys. These values were found to be close to those obtained by differential thermal analysis measurements. The lengths of the helices are strongly influenced by the deliberated heat of fusion during solidification. The substantially higher mould-filling capacity of the Ni–Cr–Be alloy compared with that of the Au–Ag–Cu alloy can be explained to a large extent by the corresponding difference in their latent heat of fusion. A calculation of the lengths of the helices requires a knowledge of the speeds of the melts. So far there are only indications of a higher speed for the Ni–Cr–Be alloy than for the Au–Ag–Cu alloy with the casting machine employed. The highest slope for the length of helix against supertemperature curve was observed for the Au–Ag–Cu alloy, indicating a smaller heat transfer coefficient for this alloy than for the Ni–Cr–Be alloy.

1. Introduction

Castability is not a specific alloy property and is usually considered to be a measure of the mould-filling capacity of the alloy. The measured values for any test pattern also depend on the machine applied and the casting conditions. In comparing alloys, all other factors should therefore be kept constant.

It is important for the interpretation of the observed castability that a mathematical relationship can be established with the contributing factors based on physical models. This goal requires a constant cross-section of the test channel and has not been achieved with the test patterns that have so far been applied in the castability testing of dental alloys. Two widely used test patterns are: (1) a polypropylene mesh screen filled by the melt [1] and (2) a cylindrical crown with a sharp margin where the castability is assessed by the degree of deficiency in reproducing the full length of the margin [2]. The castability, as measured by the mesh screen pattern, does not increase linearly with the fraction of the screen filled with metal [3]. The filling of a sharp margin has been found to be greatly hampered by back pressure from remaining mould gases [4], and the quantitative relationship between the variable temperatures and deficiencies of the margins is unknown.

In testing the castability of alloys in general, a spiral pattern with a constant wire cross-section is frequently used [5]. However, the diameter of the channel is usually larger than that typical of dental castings. The aim of this work was to cast helices of a small and constant cross-section and to analyse quantitatively the observed mould-filling capacities of two dental casting alloys.

2. Materials and methods

In this work a helix pattern was formed by winding a 0.9 mm diameter polyamide wire on an aluminium mandrel with a diameter of 29 mm as shown in Fig. 1. A track for the polyamide wire was machined on the surface of the mandrel. The wire was heat treated at 150° C for 45 min while fixed to the mandrel and was slowly cooled to room temperature in order to attain a permanent helical shape. The initial part of the wire was along the length axes of the helix as shown in Fig. 1 to produce a smooth entrance of the metal flow from the crucible former into the spiral. The polyamid helix attached to the wax for the crucible former was invested in a conventional manner with a phosphate-bonded material (Aurovest soft, BEGO, FRG).

The chemical compositions, the liquidus and solidus temperatures, as well as the density, all according to the manufacturers, of the two alloys investigated are presented in Table I. The preheating temperature of the investment mould was chosen so that a temperature difference between the liquidus temperature of the alloys according to the manufacturer and the mould temperature was 340° C in all experiments.

Five casting temperatures were used in casting the helices: the liquidus temperature and temperatures 20, 50, 70 and 100° C above the liquidus temperature (supertemperatures). Four castings were made at each temperature. The casting machine was of a vacuum–pressure type with electrical resistance heating and thermocouples in the bottom and the side walls of the furnace lining (Combilator CL-G 2002, Heraeus, FRG). A schematic drawing is shown in Fig. 2. Vacuum was applied to the crucible–mould assembly before pouring took place by turning it upside down. Within 1 sec after the tilting was finished the air pressure above the melt that had fallen into the crucible former was raised rapidly to 1 atm (about 101 kPa). The weight of each casting was 9 g for each alloy. The

0957–4530/90 $03.00 + .12

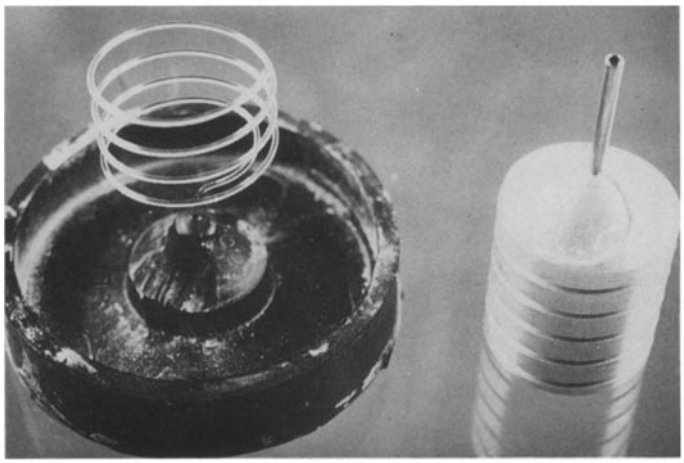

Figure 1 The mandrel of aluminium (right) with a machined track for the shaping of a spiral and a helix of a polamid wire mounted in the crucible former (left).

lengths of the cast helices were calculated on the basis of their weight, diameter and density.

In another series of experiments plates 20 mm × 20 mm × 2 mm were cast with a thermocouple positioned in the middle of the plates as shown in Fig. 3. The thermocouple was made up of 0.1 mm diameter wires of Pt/Pt–10% Rh. The extensions of the thermocouple consisted of special compensation wires (type RIS, Gordon Comp, IPP, USA). The passage of these wires from the mould to the outside of the vacuum–pressure chamber was through the hollow axes of rotation for the mould–crucible assembly. The seal consisted of epoxy around the wires in a tube at the outlet of the rotation axes. Two plates were cast of each alloy as well as for pure silver at a supertemperature of 100° C.

Differential thermal analyses (DTA) were made of each alloy for the determination of their latent heat of fusion at a cooling rate of 20° C min^{-1} in an argon–2% hydrogen atmosphere using an Al_2O_3 crucible (DSC 405, Netch Gerätebau GmbH, FRG).

3. Results

The average lengths with standard deviations of the helices for the two alloys as a function of the supertemperature at the onset of casting are shown in Fig. 4. The increase in length with the supertemperature is only moderate for both alloys. The slope was higher for the gold alloy (40 mm (100° C)$^{-1}$) than for the nickel alloy (17 mm (100° C)$^{-1}$). The mould-filling capacity of the nickel alloy was clearly superior to the gold alloy over the whole range of applied casting temperatures.

The temperature–time curves in the initial phase of the casting process for the 2 mm thick plates of two alloys are shown in Figs 5 and 6. The temperature diminishes rapidly for both alloys until a kind of a plateau is reached after about 0.5 sec for the gold alloy (Fig. 6) and after 1.5 sec for the nickel alloy (Fig. 5). The lengths of these plateaux were 19 and 21 sec for the nickel alloy and 3 and 4 sec for the gold alloy.

The heat flow is plotted against the temperature during solidification in the DTA experiments for these alloys in Figs 7 and 8. The latent heat of fusion according to these curves are given in Table I.

4. Discussion

4.1. Heat flow

The rate of heat flow from the melt to the mould is crucial for the solidification time and thus for the mould-filling capacity of the alloy. The heat flow will in principle have to cross the metal–mould interface and subsequently to pass through the investment to the outer surface of the mould. Both processes occur at the same time, but usually one of them controls the rate of heat flow. Considering the first alternative the rate of heat flow Q (J cm^{-2} sec^{-1}) across the interface for a metal at its melting point T_M is [6]

$$Q = -h(T_M - T_0) \quad (1)$$

where T_0 is the mould temperature and h is the heat transfer coefficient (J cm^{-2} °C^{-1} sec^{-1}). The temperature profile is illustrated schematically in Fig. 9. The heat crossing a flat interface comes from the heat of fusion H (J g^{-1}) since the solidifying melt is exactly at the melting point of the metal or at the liquidus

TABLE I Composition (in wt %) according to the manufacturers and physical properties of the alloys investigated.

Alloy	Name of alloy	Au	Pt	Ag	Cu	Zn	Ni	Cr	Be	Mo	T_{sol} (°C)	T_{liq} (°C)	ρ (g cm^{-3})	c_p^* (J g^{-1} °C^{-1})	$H^\dagger$ (J g^{-1})
1	Rexillium III‡						76	13	1.8	5.5	1150 1130	1290§ 1245†	7.75§	0.80	504
2	Delta 2¶	73	2.5	12.5	11.0	1.0					850 845	920§ 910†	15.4§	0.198	126

*On the basis of the specific heat and the weight fraction of each element in the alloy.
†On the basis of DTA measurements.
‡Jeneric Inc., USA.
§According to information from the manufacturers.
¶K. A. Rasmussen AS, Norway.

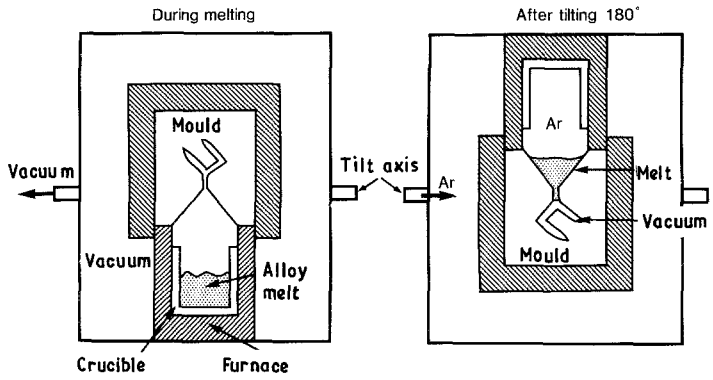

Figure 2 Schematic drawing of the applied vacuum–pressure casting machine.

temperature of the alloy

$$Q = -\rho_s H \frac{\partial S}{\partial t} = -h(T_M - T_0) \qquad (2)$$

where ρ_s is density of the metal, S is the thickness of the solidified metal and t is the time.

When the rate of heat flow is controlled by conduction through the investment, the temperature of the mould surface as an approximation is assumed to be raised suddenly from the mould temperature T_0 to T_M as the metal is poured. The temperature profiles for three different times t are shown schematically in Fig. 10. The heat flow is then of a non-stationary type and for a one-dimensional case (which is nearly correct for the present plate), it must conform with the partial differential equation

$$\frac{\partial T}{\partial t} = \alpha_m \frac{\partial^2 T}{\partial x^2} \qquad (3)$$

where α_m is the thermal diffusivity of the mould ($cm^2\ sec^{-1}$) and x is the distance (cm) from the mould wall with the positive direction into the metal. The thermal diffusivity is defined as

$$\alpha_m = K_m/\rho_m c_m \qquad (4)$$

where K_m is the thermal conductivity of the mould ($J\,cm^{-1}\,sec^{-1}\,°C^{-1}$) and c_m the specific heat of the mould ($J\,g^{-1}\,°C^{-1}$). Following [6], the solution to the differential equation (Equation 3) expressed as the rate of heat flow across a flat mould–metal interface is

$$Q = -\left(\frac{K_m \rho_m c_m}{\pi t}\right)^{1/2} (T_M - T_0) \qquad (5)$$

If the metal is at its melting point, the heat flow must come from the heat of fusion H

$$Q = -\rho_s H \frac{\partial S}{\partial t} = -\left(\frac{K_m \rho_m c_m}{\pi t}\right)^{1/2} (T_M - T_0) \qquad (6)$$

Thus, the rate of heat flow is in this case dependent on both time and temperature.

Equations 1 and 2 can be assumed to be valid in the initial part of the solidification process before the temperature of the internal surface of the mould is raised substantially above T_0 by the liquid metal. From Figs 5 and 6 it can be seen that the slope of the cooling curve is reduced continuously with time in the first part of the curve before solidification, and the liberation of latent heat of fusion commences, indicated by a discontinuity of the slope. Thus, the constant temperature difference assumed in Equations 1 and 2 is likely to exist only for the first small fraction of a second after pouring. Accordingly, the other mechanism where the rate of the heat flow is governed by conduction through the investment may be overriding in these experiments, with total solidification times of several seconds (Figs 5 and 6). This assumption is supported by the fact that the melt reacts with the investment surface, eliminating air gaps between the melt and the mould. The interface resistance to heat transfer in such cases can be expected to be low.

4.2. Heat of fusion

Equation 6 can be integrated from $S = 0$ at $t = 0$ to S for t_e at the end of the solidification

$$S = \frac{2}{\pi^{1/2}} (K_m \rho_m c_m)^{1/2} \frac{T_M - T_0}{\rho_s H} t_e^{1/2} \qquad (7)$$

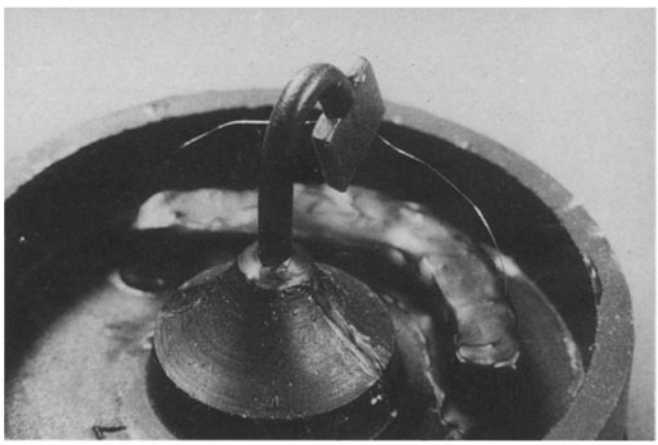

Figure 3 The wax pattern with a mounted thermocouple for the measurement of temperature against time during soldification.

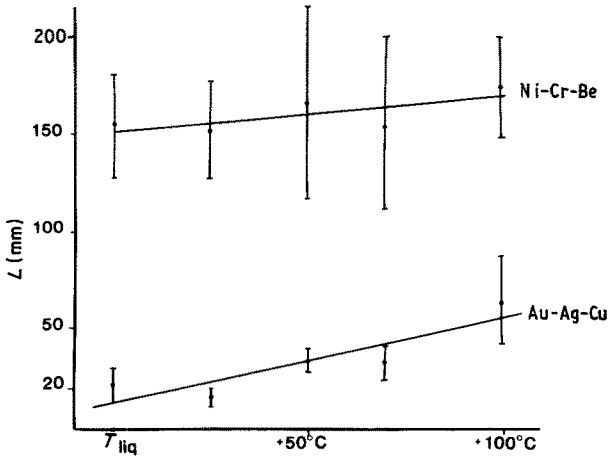

Figure 4 Average length of helices with standard deviations plotted against supertemperature for the alloys investigated.

From this equation the heat of fusion for the applied alloys can be determined if the properties of the mould material in the parentheses are known along with S and t_e. Unfortunately, no thermal property data are available for the investment material employed. However, the product in the parentheses in Equation 7 can be eliminated by measurement of the solidification time for a metal like silver with a known heat of fusion (111 J g^{-1}) [7]. Using Equation 7 the following expression is then obtained

$$\frac{H_{\text{alloy}}}{H_{\text{Ag}}} = \frac{\rho_{\text{Ag}}}{\rho_{\text{alloy}}} \left(\frac{t_e^{\text{alloy}}}{t_e^{\text{Ag}}} \right)^{1/2} \quad (8)$$

For pure silver the temperature–time curve was distinctly flat for 2.6 sec, which was taken as the total solidification time. The time for the two alloys to reach the solidus temperature t_e, i.e. 1150° C for the nickel alloy and 850° C for the gold alloy, is beyond the end of the plateaux in Figs 5 and 6 and corresponds more to a minimum in the curves dT/dt against t, i.e. $d^2T/dt^2 = 0$. The reason for this is the microsegration that takes place and the small solidification rates in the final stage [8]. The average time for the melts to reach the solidus temperatures was 5.5 and 27 sec for the two alloys. In this way the heat of fusion for the gold alloy was found to be 110 J g^{-1} and for the nickel alloy 487 J g^{-1}. These values are about 5 to 10% lower than those obtained from the DTA measurements. This can be considered satisfactory in view of the approximate model for heat flow that has been applied. These measurements and calculations support the concept of conduction through the investment as the governing step for the rate of the heat flow.

4.3. Effect of heat of fusion on the length of the cast helices

Equation 7 can be used to calculate the length of the cast helix, L, with a wire diameter $r = 0.9$ mm. For a wire with a curved instead of a flat surface, the expression obtained in Equation 7 is only an approximation. An analogous equation for a cylindrical surface is more appropriate, but this case requires that K_m be known explicitly [6]. When $L = vt_e$ and v is the average flow speed of the melt in the channel, L can be found by using Equation 7

$$t_e = \frac{L}{v} = \left(\frac{\rho_s Hr}{T_M - T_0)2} \right)^2 \frac{\pi}{K_m \rho_m c_m} \quad (9)$$

The average speeds of the melts, v, were unknown in these experiments. If they are assumed, as a first approximation, to be equal, then we obtain the ratio

$$\frac{L_{\text{Ni-alloy}}}{L_{\text{Au-alloy}}} = \left(\frac{\rho_{\text{Ni-alloy}} H_{\text{Ni-alloy}}}{\rho_{\text{Au-alloy}} H_{\text{Au-alloy}}} \right)^2 \quad (10)$$

Using the heat of fusion values achieved in this work, this ratio of the lengths of the helices is calculated to be 5.0 compared with an observed ratio of 7.1 for zero superheat (Fig. 4). Thus, the substantial difference in the heat of fusion between the alloys can to a large extent explain the superior mould-filling capacity of the nickel alloy compared with the gold alloy, in spite of its lower density (Table I). The heat of fusion per cm^3 in Equation 9 (ρH) is 3776 J cm^{-3} for the nickel alloy and 1462 J cm^{-3} for the gold alloy.

In addition comes the energy dissipated due to the heat capacity of the solid plus liquid metal during the temperature drop T^1 of the alloy from the solidus to the liquidus temperature ($\rho c T^1$). The heat capacity c of the two alloys can be calculated to be 0.197 J g^{-1} °C^{-1} (gold alloy) and 0.80 J g^{-1} °C^{-1} (nickel alloy) on the basis of c-values for the individual metal components and a weighted average for the alloys [9]. For the nickel alloy and the gold alloy the dissipated heat due to their heat capacity is then 710 and 168 J cm^{-3}, respectively. If these values are added to the H-values in Equation 9, the calculated ratio for the length of the helices is 5.8, which is even closer to the observed value.

The plot of ΔL against ΔT can be extrapolated to a

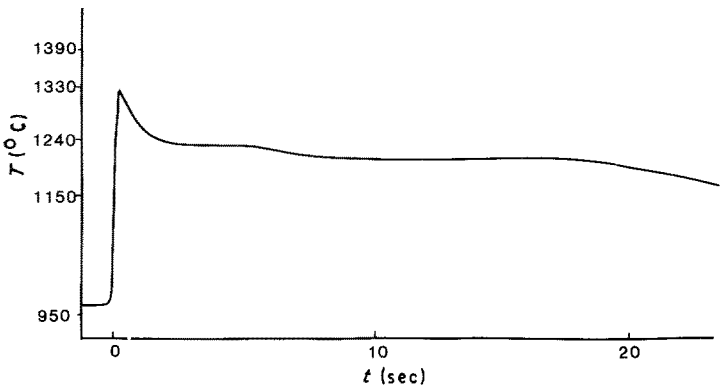

Figure 5 Temperature–time plot during solidification for the Ni–Cr–Be alloy.

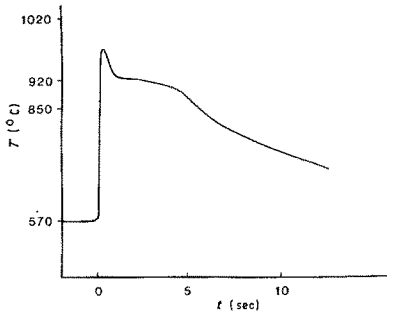

Figure 6 Temperature–time plot during solidification for the gold alloy.

45° C lower temperature for the nickel alloy because of an observed T_{liq} = 1245° C in the DTA experiments compared with 1290° C as claimed by the manufacturer (Table I). The length of the cast helix is then reduced from 156 to 146 mm and the ratio in Equation 9 is thereby lowered to 6.6, which is more in line with the calculated value of 5.8.

4.4. Speeds of the melts

Since the observed ratio of the length of the helices was found to be slightly higher than the calculated value, it is reasonable also to focus on the average speeds of the melts, v (Equation 9). The ratio of the length of the helices indicates that the speed of the melt of the nickel alloy can be expected to be higher than for the gold alloy. Assuming t_e to be independent of v, an estimation of v can be made by the relationship $v = L/t_e$. This requires that t_e can be found for a 0.9 mm diameter wire of the two alloys. Equation 9 can be applied for this purpose, using the observed t_e-values for the 2 mm thick plate to determine the product of all variables other than r on the right-hand side of Equation 9. The solidification times t_e for a 0.9 mm diameter wire are then calculated to be 1.1 and 5.5 sec, respectively, for the gold and nickel alloys. Using the observed lengths of the helices (15 and 146 mm for zero superheat; Fig. 4), the average speed of the melts are calculated to be 13.5 and 27.5 mm sec^{-1}. These values thus indicate a higher average speed for the melt of the nickel alloy than for the gold alloy, as anticipated. If the ratio of the average speeds of the alloys are included in Equation 10, then the calculated

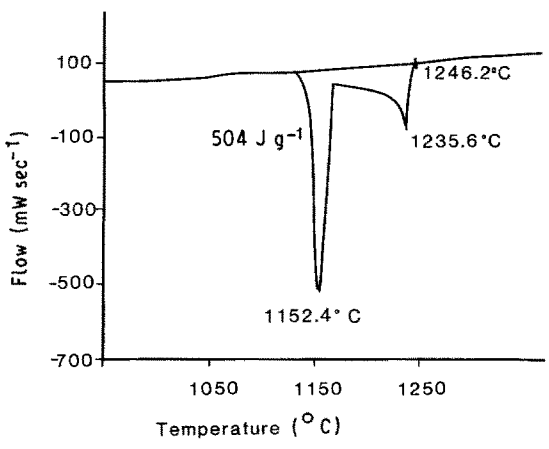

Figure 7 Heat flow plotted against temperature during solidification in the DTA experiments for the Ni–Cr–Be alloy.

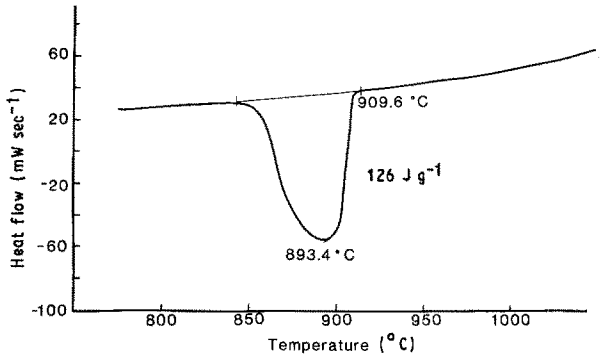

Figure 8 Heat flow plotted against temperature during solidification in the DTA experiments for the gold alloy.

ratio of the helix lengths will be 10.0 and thus higher than that observed.

The initial speed is continuously reduced as the alloy flows into the mould channel, due to friction between the melt and the walls of the channel. The solidified metal on the walls usually has a rough rather than a smooth surface because of dendrites protruding into the melt. The surface roughness is generally more severe for alloys than for pure metals and for alloys of a eutectic composition. The reason is that constitutional supercooling, which promotes dendrite formation, does not occur for the two latter cases. A corresponding superior castability has been observed [9]. In this context it is interesting to note that the nickel alloy is partially eutectic [10]. About 60% of the latent heat of fusion derives from this fraction of the structure according to the area under the last peak in the heat flow against temperature diagram (DTA) in Fig. 7. Further metallographic studies of the solidification front are necessary for a more detailed discussion of this topic.

The initial speed of the melt, v_0, can be calculated according to Bernoulli's equation [11]

$$v_0 = 2\frac{P - P_0}{\rho} + 2gy \qquad (11)$$

where $P = P_0$ is the pressure difference, equal to 1 atm (about 101 kPa) in the present experiments, and y is the height of the melt. The first term on the right-hand side is dominating for the small melts

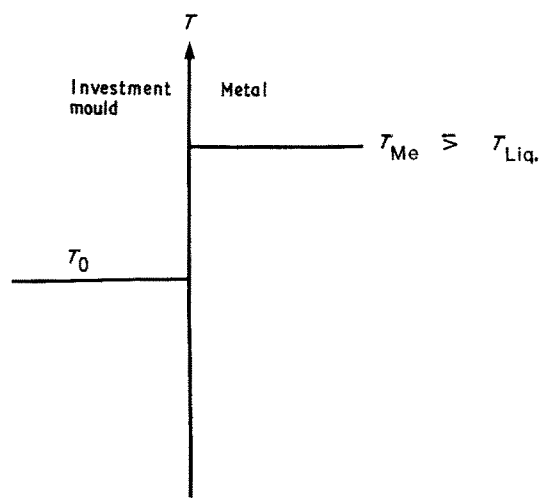

Figure 9 Schematic diagram of the temperature-profiles during casting. Heat flow controlled by the metal–mould interface resistance.

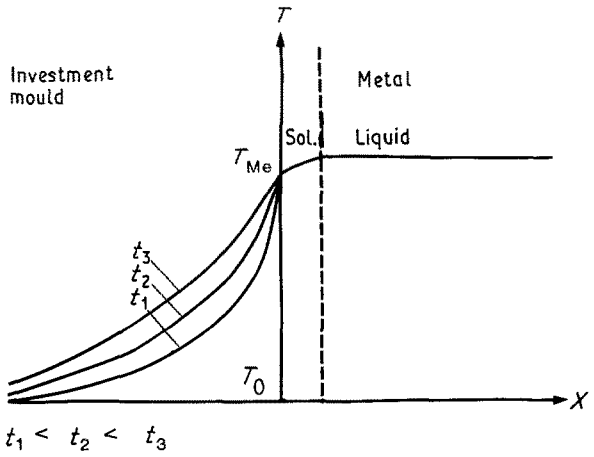

Figure 10 Schematic diagram of the temperature-profiles during casting. Heat flow controlled by conduction through the investment. Temperature profiles at three different times t.

applied in these investigations. The initial speeds for the melts of the nickel and the gold alloys are then calculated to be 5100 and 3600 mm sec^{-1}, respectively. The difference is due to the density of the two alloys. The ranking of speeds of the alloys is the same as for the average speed values. However, the initial values are about 20 times larger than the average calculated speeds on the basis of ΔL and t_e, and indicate a substantial speed reduction during the flow of the melt due to friction and narrowing of the channels because of solidification.

4.5. Effect of supertemperature on the length of the cast helices

The slope of the plot of helix length against supertemperature ΔT (Fig. 4) was found to be larger for the gold alloy than for the nickel alloy. In this initial stage of the mould filling the heat flow is likely to be controlled primarily by the heat transfer across the interface of the alloy–investment. The heat flow in Equation 1 now derives from the heat capacity, c, of the superheated metal. According to [6] the following equation is obtained for the increased helix length ΔL due to supertemperature

$$\Delta L = \Delta T r \rho c v / 2h(T_i - T_0) \qquad (12)$$

where T_i is the temperature of the melt as it enters the mould. The slope will then be

$$\frac{d(\Delta L)}{d(\Delta T)} = \frac{r\rho cv}{2h(T_i - T_0)} \qquad (13)$$

If $T_i - T_0$ is approximately equal for the two alloys before the start of solidification, $d(\Delta L)/d(\Delta T)$ will vary with $\rho cv/h$. The calculated heat capacity was almost four times higher for the nickel alloy than for the gold alloy (Table I) and the speed of the nickel alloy has been estimated to be higher. On the other hand, the density is about twice as high for the gold alloy as for the nickel alloy. Nevertheless, the product ρcv should be largest for the nickel alloy. The steeper slope for the gold alloy thus indicates a smaller heat transfer coefficient, h, for this alloy for the nickel alloy.

Acknowledgements

The author expresses his gratitude to Mr P. A. Sunnerkrantz for his assistance with the temperature–time measurements during solidification and to Netch Gerätebau GmbH, (FRG) for carrying out the DTA measurements.

References

1. R. P. WHITLOCK, R. W. HINMAN, G. T. EDEN, G. DICKSON and E. E. PARRY, *J. Dent. Res.* **60** (Special Issue A) (1981) 74.
2. P. J. BROCKHURST, U. G. McLAVERTY and Z. KASLOFF, *Oper. Dent.* **8** (1983) 130.
3. S. HIRANO, J. A. TESK, R. W. HINMAN, H. ARGENTAR and T. M. GREGORY, *Dent. Mater.* **3** (1987) 307.
4. M. C. FLEMINGS, "Solidification Processing" (McGraw-Hill, New York, 1974) p. 221.
5. *Idem, ibid.* p. 219.
6. *Idem, ibid.* p. 13.
7. R. C. WEAST (editor), "Handbook of Chemistry and Physics", 66th Edn (CRC Press, Boca Raton, Florida, 1986) p. D185.
8. H. FREDRIKSSON and B. ROGBERG, *Met. Sci.* (December 1979) 685.
9. M. C. FLEMINGS, "Solidification Processing" (McGraw-Hill, New York, 1974) p. 222.
10. H. HERØ, E. SØRBRØDEN and J. GJØNNES, *J. Mater. Sci.* **22** (1987) 2542.
11. F. W. SEARS, M. N. ZEMANSKY and H. D. YOUNG, "University Physics", 7 Edn (Addision-Wesley, Reading, Massachusetts, 1987) p. 322.

Received 6 November
and accepted 13 November 1989